Paper No.
7183

NACE INTERNATIONAL CORROSION 2016 CONFERENCE & EXPO

Sour Service Fatigue and Fracture Behavior of High Strength Steels

Ramgopal Thodla[*], Jeffery Hawk[**], Margaret Ziomek-Moroz[**]
[*]: DNV GL USA 5777 Frantz Road, Dublin, OH - 43017
[**]: NETL 1450 Queen Avenue SW, Albany, OR 97321-2198

ABSTRACT

Fatigue Crack Growth Rate (FCGR) and fracture toughness behavior of high strength steels used in drilling riser applications was investigated in sour environments. Frequency scan tests were performed were performed on API[*] 5L X80 (X80), API 5CT C110 (C110), and API 5DP S135 (S135) in moderate to mildly sour environments. Fatigue crack growth rate increased with decreasing frequency and reached a plateau value at low frequencies. The observed behavior is typical for hydrogen enhanced cracking in sour environment. The rate controlling step for FCGR was found to be hydrogen diffusion through the fracture process zone. The critical concentration for crack advance was calculated based on a model based on hydrogen diffusion through the fracture process zone. The critical concentration of hydrogen for S-135 was significantly lower than C-110, and X-80. The critical concentration of hydrogen for crack advance for C-110, and X-80 were similar. Rising-displacement FT tests were performed in a range of environments to determine the resistance (R-curve) behavior. Tests were performed in-situ at a slow K rate of 0.05Nmm$^{-3/2}$/s over a range of environmental conditions as well as microstructures, namely, S-135, C-110, X-80. The results show that the initiation toughness, and the slope of the R-curve decreased sharply in the sour environments.

INTRODUCTION

Offshore HP/HT flow lines are subject to large thermal transients particularly during shut down. These thermal transients tend to vary from about 200°F to ambient temperature and place a large fatigue demand on the pipelines. The transients typically are very low frequency events with high amplitudes, which can lead to lateral buckling. The loading rates associated with the transients are very slow, hence the toughness properties of the material in environments at low loading rates are important. The pipelines are also subject to high stress and thus need to have good toughness properties. Risers are also subject to significant fatigue loading, though under conditions different from flow lines, typically they are subjected to fatigue loading at higher frequencies.

Significant amount of work have been performed in sour service environments to understand the performance of carbon steels in dynamic applications like risers and flow lines. The effect of H_2S on steels is typically observed as an increase in the fatigue crack growth rate (FCGR), with FCGR at high ΔK values being as high as 50x the values in-air. FCGR studies in a range of environments indicate that FCGR increases with increasing H_2S concentration.[1-5] Another important effect in sour environments on FCGR is the effect of cycle frequency. Usually it is

[*] American Petroleum Institute

©2016 by NACE International.
Requests for permission to publish this manuscript in any form, in part or in whole, must be in writing to
NACE International, Publications Division, 15835 Park Ten Place, Houston, Texas 77084.
The material presented and the views expressed in this paper are solely those of the author(s) and are not necessarily endorsed by the Association.

found that the FCGR increases with decreasing frequency and reaches a plateau at low frequency.[6-9] More recent data on reeled pipe (pipe with 1.5% strain) has explored the effect of frequency on FCGR[9]. As with other FCGR data, the FCGR increases with decreasing frequency and reaches a plateau. Typically in low pH environments containing H_2S, the FCGR increases with decreasing frequency and quickly reaches a plateau at relatively high frequencies of about 1Hz to 0.3Hz. This is most likely associated with the possibility that high corrosion rates at low pH could lead to crack tip blunting and/or formation of voluminous corrosion products that lead to crack closure[10]. The lower H_2S concentration also leads to a lower concentration of hydrogen in the metal and hence the lower values of FCGR[10,11].

Sour Service FCGR appears to be largely influenced by the hydrogen content in the metal. In sour environments there are two primary sources of hydrogen

a) Hydrogen due to bulk dissolution of the steel and subsequent ingress of hydrogen into the metal
b) Charging of hydrogen from the crack tip due to local dissolution at the crack tip system.

Uncoated samples have a higher FCGR, suggesting that the bulk hydrogen is the primary driver for FCGR and the crack tip hydrogen does not play as critical a role in the process[9]. The FCGR frequency scan data over a range of conditions can broadly be described as increasing FCGR with decreasing frequency, and reaching a plateau value at lower frequencies. Another general observation is the fact that in the higher frequency regime, the FCGR has a $1/\sqrt{f}$ dependence which is consistent with a hydrogen diffusion based mechanism.

EXPERIMENTAL

FCGR and fracture toughness experiments in a range of sour environments were performed on three different materials S-135, C-110, and X-80 with nominal YS of 135ksi/110ksi/ and 80ksi respectively. Samples were machined from the steel pipes in the L-C orientation with the notch running through thickness. The specimens were machined with a notch and pre-cracked to an a/W of 0.35 at a ΔK of $522 Nmm^{-3/2}$. Fracture toughness tests were performed on SENB specimens, the specimens were pre-cracked to a final a/W of 0.5. The SENB specimens were B×2B samples with a B = 0.3". FCGR tests were performed on CT specimens.

Hydrogen flux measurements were performed using the Devanathan cell. Test specimens of 2.5" by 2.5" by 1mm were exposed one side of the specimen exposed to the sour environment and the hydrogen flux exiting from the specimen was measured One side of the sample was exposed to the sour service, while the other side of the specimen was polarized to +300mV SCE in 0.1M NaOH to oxidize the hydrogen that was exiting through the specimen. The current transient measured represents the flux of hydrogen that is egressing from the specimen.

Test Matrix

The tests in the current test program involved the following:

a) Hydrogen Flux Measurements using the Devanathan Cell & Thermal Desorption Analysis.
b) Fatigue Crack Growth Rate Testing
c) Fracture Toughness Testing

All flux measurements were performed in a solution containing 5wt% NaCl. The test matrix for the various materials is shown in Table 1. Thermal desorption studies were performed on all of the materials after cathodically charging with hydrogen. Samples from every steel grade were

©2016 by NACE International.
Requests for permission to publish this manuscript in any form, in part or in whole, must be in writing to
NACE International, Publications Division, 15835 Park Ten Place, Houston, Texas 77084.
The material presented and the views expressed in this paper are solely those of the author(s) and are not necessarily endorsed by the Association.

charged during different times (1, 2, 4, 6 and 8h) in a 1M H_2SO_4 solution with 10mg/l thiourea with a constant current of 1mA/cm² (galvanostatic). The resulting hydrogen was measured and it was found that there was no significant change in hydrogen concentration after charging for 2h. Hence all samples were charged for 2h after which thermal desorption analysis was performed. Thermal desorption spectra were obtained at three different ramp rates of 400°C/h, 800°C/h, and 1200°C/h.

All FCGR and FT tests were performed in a solution which contained 5wt% NaCl, the test matrix is shown in Table 1. All faces of the CT and SENB specimens, were exposed to the environment to maximize the concentration of hydrogen in the test specimen. All test specimens were exposed to the test environment for 4 days prior to beginning testing.

FCGR frequency scan tests were performed at a constant ΔK ranging from 606 to 1211Nmm$^{-3/2}$. The test frequency was varied from 1Hz to 1mHz. Crack length was measured as a function of time, typically at each frequency the crack growth was between 0.5mm to 1mm. FT tests were performed as rising displacement tests with an initial nominal K-rate of 0.05Nmm$^{-3/2}$/s.

RESULTS AND DISCUSSION

Hydrogen Flux Measurements

The results of the hydrogen flux measurements performed on UD-165 and S-135 with specimens exposed to sour service at pH = 6 and 7 are shown in Figure 1:. Hydrogen is generated on the sour environment side of the specimen and ingresses into the steel, however with time there is a build-up of FeS scale which leads to a decrease in the corrosion rate and hence a lower concentration of hydrogen with time as the film builds. It is interesting to note that the hydrogen flux in S-135 is very low for all environments except pH = 7, p_{H2S} = 0.12psia. The results of the hydrogen flux measurements performed on C-110 and X-80 at pH = 4 and 5 are shown in Figure 2:. Similar to the tests performed on the higher strength steels of UD-165 and S-135 there is a build-up of FeS scale which leads to a decrease in the hydrogen flux.

The diffusion co-efficient is estimated from the time for hydrogen to break through based on equation [1][13].

$$D_{eff} = \frac{L^2}{15.3 t_{breakthrough}} \qquad [1]$$

where :

D_{eff} - Effective diffusion coefficient (cm^2/s)
L - Sample thickness (cm)
$t_{breakthrough}$ - Elapsed time before hydrogen breaks through on the exit side

The subsurface concentration of hydrogen was estimated using equation [2]

$$C_s = J_{ss} L / D_{H,eff} \qquad [2]$$

Where:
C_{ss} – Subsurface concentration (mol/cm^3)
J_{ss} - Steady state hydrogen flux (mol/cm^2-s)

©2016 by NACE International.
Requests for permission to publish this manuscript in any form, in part or in whole, must be in writing to
NACE International, Publications Division, 15835 Park Ten Place, Houston, Texas 77084.
The material presented and the views expressed in this paper are solely those of the author(s) and are not necessarily endorsed by the Association.

The concentration of diffusible hydrogen and the effective diffusion co-efficient of hydrogen is shown in Table 2. The effective diffusion co-efficient of hydrogen for S-135 and UD-165 was in the range of 1×10^{-8} cm^2/s to 6×10^{-9} cm^2/s, while the effective diffusion co-efficient of hydrogen for C-110 and X-80 are in the range of 5×10^{-8} cm^2/s and 1.5×10^{-7} cm^2/s respectively. The concentration of diffusible hydrogen for S-135 and UD-165 are higher at pH = 6 and are in the range of 1×10^{-4} mol/cm^3. At the higher pH of 7, the concentration of hydrogen drops sharply to about 5×10^{-6} mol/cm^3. This is likely because at pH 7 the corrosion rate of steels decreases as well as the speciation of H_2S changes and is in the form of SH^-. This is a likely reason for the lower hydrogen concentration at pH 7. The concentration of diffusible hydrogen for C-110 and X80 is in the range of 2×10^{-4} mol/cm^3 at pH 4 and 5.

It is clear from the hydrogen flux measurements that the diffusion co-efficient of the higher strength steels is in the range of 1×10^{-8} cm^2/s to 6×10^{-9} cm^2/s, while the lower strength steels are in the range of 5×10^{-8} cm^2/s and 1.5×10^{-7} cm^2/s. This is consistent with the data in literature where the diffusion co-efficient of hydrogen in high strength quenched and tempered martensitic steels was measured to be the range of 10^{-8} cm^2/s. The lower strength C-110 steel has a slightly higher diffusion co-efficient, while the line pipe steel X80 has a diffusion co-efficient of hydrogen of 1.5×10^{-7} cm^2/s which is consistent with measurements on line pipe steels.

The concentration of diffusible hydrogen for the higher strength steels (UD1-65 and S-135) in acidic environments (pH below 7) is largely independent of the H_2S concentration at the levels investigated. This is observed even for C-110 and X80 steels at pH 4 and 5, where the concentration of diffusible hydrogen is independent of the H_2S concentration as well as the pH in this range. This is likely due to the fact that the corrosion rate of the steels in these ranges of the environments do not vary strongly with the pH and H_2S. The formation of FeS likely controls the corrosion rate and hence the hydrogen ingress.

Thermal Desorption Analysis

Thermal desorption analysis were performed on four different steels after cathodically charging with hydrogen. The analysis of the peaks was performed assuming that the hydrogen in the trap sites (A) were in equilibrium with normal interstitial sites (B). The activation energy (E_a), needed for the H to escape from a trapping site is much higher than that of normal lattice diffusion (E_n). An analysis of the maximum escape rate is determined by minimizing dx/dt and the resulting solution relates the activation energy for hydrogen desorption with the heating rate and the temperature at which the peak in hydrogen desorption occurs. The equation describing the relationship is shown below in equation [3]:

$$\frac{\partial(\ln(\phi / T_c^2)}{\partial(1/T_c)} = -E_a / RT \qquad [4]$$

where

- ϕ: Heating rate
- T_c: Temperature at which maximum in the hydrogen desorption peak
- E_a: Activation energy (kJ/mole)
- R: Gas constant
- T: Temperature (K)

©2016 by NACE International.
Requests for permission to publish this manuscript in any form, in part or in whole, must be in writing to
NACE International, Publications Division, 15835 Park Ten Place, Houston, Texas 77084.
The material presented and the views expressed in this paper are solely those of the author(s) and are not necessarily endorsed by the Association.

Figure 3: shows the plot of $\frac{\partial(\ln(\phi / T_c^2)}{\partial(1/T_c)}$ vs *1/T* for the various steels studied. The slope of the lines represents the activation energy. C-110 and X80 have two peaks and the activation energies. The activation energy for the various steels is shown in Figure 3:. The activation energy of UD-165 and S-135 is 34kJ/mole and 38kJ/mole, while the activation energy of C-110, and X80 are 48kJ/mole and 27kJ/mole respectively. The activation energy corresponding to the secondary peaks in C-110 and X80 desorption spectra are 67kJ/mole and 43kJ/mole.

The activation energy obtained from the thermal desorption analysis was used to determine the number of reversible trap sites. The measured effective diffusion co-efficient can be expressed as

$$D_{eff} = D_o N_l / N_r \exp(-E_a / RT) \qquad [5]$$

where

- D_{eff}: Effective diffusion co-efficient of hydrogen
- D_o: Lattice diffusion co-efficient of hydrogen (7.23×10^{-4}cm^2/s)[14]
- N_l: Number of lattice sites in the steel (5.23×10^{23}sites/cm^3)[15]
- N_r: Number of reversible sites

The number of reversible traps associated with the higher strength steels is on the order of 10^{22}sites/cm^3 which is likely because of the higher number of interfaces where the hydrogen can be trapped compared to C-110. In case of X80 the number of reversible trap sites for hydrogen is lower than reported for similar steels like API 5L X70[16]. In X70 the trap binding energy was measured by measuring hydrogen flux measurements at different temperatures giving a binding energy of about 36kJ/mole[16], which may be a composite binding energy associated with two different sets of trap sites. In the current work two different trap binding energies were identified and is likely the cause for the difference between the estimated number of trap sites.

Fracture Toughness Results

The J-R curve of three different steels in air is shown in Figure 4: The R-curves exhibit a smooth behavior with S-135 exhibiting the lowest R-curve behavior. Figure 4: also shows the R-curve behavior of four different steels in a set of sour environments. UD-165™ and S-135 were tested at pH 7 at two different levels of H_2S (0.12psia and 1.2psia). C-110 and X80 were tested at pH 5 at two different levels of H_2S (0.12psia and 1.2psia). It is clear from the R-curves that the R-curves at the higher concentration of H_2S are lower than the R-curves at low concentrations of H_2S. Another interesting aspect to note is that S-135 at pH 7 with 1.2psia H_2S has very low fracture toughness with a flat R-curve, while the higher strength UD-165 doesn't exhibit flat R-curve behavior even at the higher H_2S concentration.

The R-curve behavior of C-110 at pH 5 exhibits a similar trend with H_2S concentration with the R-curve in higher concentration of H_2S exhibiting lower behavior. The effect of H_2S concentration on the R-curve behavior exhibits a similar trend although the extent of effect is significantly smaller than on C-110. Another interesting aspect to note is although C-110 has higher yield strength than X80, it exhibits higher R-curve behavior than X80.

A summary of the measured parameters associated with the R-curves are shown in Table 3. While the bulk concentration of hydrogen is important the more critical parameter is the concentration of hydrogen at the crack-tip. The concentration of hydrogen at the crack tip is enhanced due to the hydrostatic stress and is given by the expression

©2016 by NACE International.
Requests for permission to publish this manuscript in any form, in part or in whole, must be in writing to
NACE International, Publications Division, 15835 Park Ten Place, Houston, Texas 77084.
The material presented and the views expressed in this paper are solely those of the author(s) and are not necessarily endorsed by the Association.

$$C_{H,CT} = C_{H,diff} \exp(\sigma_H V_H / RT) \qquad [6]$$

where

$C_{H,CT}$:	Crack tip hydrogen
σ_H :	Hydrostatic stress ($3\sigma_{YS}$)
V_H :	Atomic volume of hydrogen in Fe ($2cm^3$/mol)

It is important to note that for the same bulk concentration of hydrogen the concentration of hydrogen is higher for a higher YS material. The relation between the crack tip hydrogen and $J_{0.2mm}$, $J_{maxload}$, A for UD-165 and S-135 is shown in Figure 5: It is clear that the $J_{0.2mm}$ associated with crack initiation as well as the pre-exponent of the power law fit (A) which is associated with toughness at 1mm decreases with increasing concentration of hydrogen at the crack tip. The relationship between the crack tip hydrogen and $J_{0.2mm}$, $J_{maxload}$, A for C-110, and X80 is shown in Figure 5: There doesn't appear to be a strong co-relation between the crack tip hydrogen and the fracture toughness parameters. The reason for the lack of relation between the fracture toughness of the lower strength steels and the crack tip hydrogen is not clear.

Fatigue Crack Growth Rate Results

The fatigue crack growth rate (FCGR) was measured in a range of environments and in a range of conditions. The results of the frequency scan on X80 at pH 5 and 0.12psia/1.2psia H_2S is shown in Figure 6:. The FCGR increases with decreasing frequency and reaches a plateau. This is behavior is consistent at the three different ΔK's the tests were performed. The absolute value of the plateau FCGR increases with increasing ΔK. The plateau values as a function of ΔK for the two different conditions are shown in Figure 7:. The plateau FCGR has a ΔK^3 dependence and is not strongly dependent on the environmental conditions.

The results of the frequency scan on C-110 at pH 5 and 0.12psia/1.2psia H_2S is shown in Figure 8:. The FCGR increases with decreasing frequency and reaches a plateau. The frequency scan behavior is similar to X80. This is behavior is consistent at the three different ΔK's the tests were performed. The absolute value of the plateau FCGR increases with increasing ΔK. The plateau values as a function of ΔK for the two different conditions are shown in Figure 9:. The plateau FCGR at pH = 5 and 0.12psia H_2S is slightly lower than in the other conditions. The plateau FCGR decreases with ΔK and has a dependence of ΔK^2 to ΔK^3.

The results of the frequency scan on S-135 at pH 7 at 0.12psia/1.2psia H_2S is shown in Figure 10:. The results of the frequency scan on S-135 at pH 6 at 1.2psia H_2S is shown in Figure 11:. The frequency scan results are similar to the data on X80 and C-110 with FCGR increasing with decreasing frequency and reaching a plateau. The absolute value of the plateau FCGR increases with increasing ΔK. The plateau values as a function of ΔK for the two different conditions are shown in Figure 10: and Figure 11:. The plateau FCGR at pH6 is significantly higher than at pH 7 over all the ΔK's studied.

It is generally accepted that fatigue crack growth of steels in sour environments is a hydrogen enhanced mechanism.[1,5,7,9] The role of bulk charging versus crack tip hydrogen has been investigated in a range of sour environments and it was shown that bulk charging of hydrogen plays a dominant role in crack propagation as opposed to crack tip hydrogen generation.[9] Diffusion of hydrogen through the fracture process zone is a time dependent process and crack advance occurs via diffusion of hydrogen through a critical distance associated with the fracture

©2016 by NACE International.
Requests for permission to publish this manuscript in any form, in part or in whole, must be in writing to
NACE International, Publications Division, 15835 Park Ten Place, Houston, Texas 77084.
The material presented and the views expressed in this paper are solely those of the author(s) and are not necessarily endorsed by the Association.

process zone. At high frequencies there is not sufficient time in a single cycle for hydrogen to travel through the critical distance. However with decreasing frequency (increasing cycle time) hydrogen can diffuse further through the process zone and at sufficiently low frequencies hydrogen diffusion can occur through the entire fracture process zone and result in crack advance through the entire fracture process zone in one cycle. At frequencies lower than this frequency there is no dependence of FCGR on the cycle frequency. The plateau FCGR is then described by the crack advancing a critical distance Δa^* in one cycle,[19-20] the crack advance being controlled by the diffusion of hydrogen. The $da/dN_{plateau}$ is described by equation [7]:

$$da/dN_{plateau} = (2/N_{crit})(\sqrt{D_{eff}/f}_{plateau})erf^{-1}(1 - C_C/C_{H,CT}) \qquad [7]$$

Where:

$da/dN_{plateau}$:	Plateau FCGR
N_{crit}:	Number of cycles to travel through the fracture process zone
D_{eff}:	Effective diffusion co-efficient of hydrogen
$f_{plateau}$:	Plateau frequency
C_c:	Critical concentration of hydrogen needed to cause damage
$C_{H,CT}$:	Concentration of hydrogen at the crack tip.

The KDF for various microstructures and in the various environments were fitted to a power law described in equation [8] over the frequency range of 1Hz to 10mHz.

$$KDF = Af^n \qquad [8]$$

Where *f*: frequency (Hz)

The plateau frequency for each frequency scan was determined by extrapolating equation [7] to the maximum KDF measured for that frequency scan. This would represent the highest frequency below which the FCGR would be independent of the cyclic frequency.

The strong dependence of FCGR on frequency where FCGR increases with decreasing frequency suggests that diffusion of hydrogen through the fracture process zone is the limiting process that controls the FCGR. It is reasonable to assume that the critical diffusion distance that hydrogen has to travel to cause damage is approximately $2CTOD_{cyclic}$ and that crack advance occurs due to diffusion of hydrogen through the fracture process zone. The critical diffusion distance of $2CTOD_{cyclic}$ for hydrogen diffusion is proposed based on modeling that has been performed by Sofronis et.al.,[18] which suggests that the peak hydrogen flux under an applied stress occurs at a distance of 2CTOD under static loads. While there hasn't been any modeling in the presence of cyclic loading it is reasonable to assume that the peak in hydrogen concentration is likely very closely related to the cyclic CTOD. It is important to realize that the exact size of the fracture zone is not critical as much as rationalizing its relation to $CTOD_{cyclic}$. The equation for $2CTOD_{cyclic}$ used is shown below in equation [9]:

$$2CTOD_{cyclic} = 2 \times (\Delta K)^2 / \sigma_{YS} E \qquad [9]$$

where σ_{YS}, the YS.

This value of $2CTOD_{cyclic}$ was used to estimate the number of critical cycles based on the plateau FCGR for each of the conditions. Earlier work in literature on various alloy systems including steels has established even though the da/dN vs frequency did not have $1/\sqrt{f}$ dependence the plateau FCGR vs $f_{plateau}$ for constant R-ratio at different ΔK did have a $1/\sqrt{f_{plateau}}$.[20] The maximum KDF as a function of plateau frequency for X80 and C-110 is shown

©2016 by NACE International.
Requests for permission to publish this manuscript in any form, in part or in whole, must be in writing to
NACE International, Publications Division, 15835 Park Ten Place, Houston, Texas 77084.
The material presented and the views expressed in this paper are solely those of the author(s) and are not necessarily endorsed by the Association.

in Figure 12:. FCGR has a $1/\sqrt{f_{pl}}$ over a range of plateau frequencies which would be consistent with hypothesis leading to equation [10]. The slope da/dN vs $1/\sqrt{f_{pl}}$ was used to estimate the critical value of hydrogen for crack advance. The N_{crit} was estimated by assuming that the critical distance for hydrogen diffusion is $2CTOD_{cyclic}$

$$da / dN = 2CTOD_{cyclic} / N_{crit} \qquad [10]$$

The average number of cycles for each environmental condition was used to estimate the critical concentration based on equation [10]. The concentration of hydrogen at the crack tip was assumed to be enhanced due to the hydrostatic stress as described by equation [6].

The result of S-135 are shown in Figure 13:, at pH 7 the plateau FCGR has a $1/\sqrt{f_{pl}}$ dependence while at pH 6 the FCGR has a ~1/*f* dependence suggesting that for S-135 there may be K1SCC behavior under these conditions. Only the data a pH 7 was utilized in performing the analysis to estimate the critical concentration for crack advance. The critical concentration of hydrogen as a function of yield strength is shown in Figure 14:. The critical concentration for crack advance for X80 and C-110 are similar, while the critical concentration for S-135 is significantly lower (~10x lower).

SUMMARY

- Hydrogen flux measurements were performed to determine the diffusion co-efficient of hydrogen as well as the concentration of diffusible hydrogen. The diffusion co-efficient of hydrogen $D_{H,UD165}<D_{H,S135}$ and $D_{H,C110}<D_{H,X80}$ under similar environmental conditions. The concentration of diffusible hydrogen in X80 and C-110 are similar. Thermal desorption studies were performed on the various steels and the binding energy associated with hydrogen was determined. The binding energy of UD-165 and S-135 are similar 34 and 38kJ/mole respectively. Hydrogen binding energy in C-110, and X80 was 48kJ/mole and 27kJ/mole respectively.
- Fracture toughness measurements were performed in a range of sour service conditions as a function of yield strength. Fracture toughness tests on sour environments exhibited a decrease compared to the in-air values. Fracture toughness parameters of crack initiation and tearing modulus were largely independent of the environment.
- Fatigue crack growth frequency scan tests performed on X80, C-110, and S-135 in a range of environments. FCGR increased with decreasing frequency before reaching a plateau in all cases. The FCGR exhibited a$1/\sqrt{f}$ dependence in all conditions suggesting that hydrogen diffusion was likely the rate limiting step.
- The plateau FCGR had a $1/\sqrt{f_{pl}}$ and was used to estimate the critical concentration of hydrogen for crack advance, the critical concentration for crack advance for X80, and C-110 were similar to each other but significantly higher than the S-135.

REFERENCES

1. Webster S E, Austen I M and Rudd W J, ‘Fatigue, corrosion fatigue and stress corrosion of steels for offshore structures’, ECSC Report No. EUR 9460, ECSC Steel Publications, European Commission, Brussels, 1985.
2. Bristoll P and Roeleveld J, ‘Fatigue of offshore structures: effect of seawater on crack propagation in structural steel', Proc. Conf. 'European Offshore Steels Research’, ECSC, 1978.
3. Eadie R C and Szklarz K E, ‘Fatigue initiation and crack closure of low alloy steels in sour brine environments’, Paper No. 610, Proc. Corrosion 99, NACE International, Houston, TX, 1999.

©2016 by NACE International.
Requests for permission to publish this manuscript in any form, in part or in whole, must be in writing to
NACE International, Publications Division, 15835 Park Ten Place, Houston, Texas 77084.
The material presented and the views expressed in this paper are solely those of the author(s) and are not necessarily endorsed by the Association.

4. Eadie R C and Szklarz K E, ‘Fatigue crack propagation and fracture in sour dilute brine’, Paper No. 611, Proc. Corrosion 99, NACE International, Houston, TX, 1999.
5. S J Maddox, R J Pargeter and P Woollin, ‘Corrosion fatigue of welded C-Mn steel risers for deepwater applications: a state of the art review’ Paper OMAE2005-67499, 24th International Conference on Mechanics and Arctic Engineering (OMAE 2005) Halkidiki Greece, 12-16 June 2005.
6. Eadie R L et al.: 'Corrosion fatigue and near-neutral pH stress corrosion cracking of pipeline steel in very dilute carbonate/bicarbonate with and without the presence of hydrogen sulfide using the compliance technique', Paper No. 03527, Proc. Corrosion 2003, NACE International, Houston, TX, 2003.
7. Buitrago J et al.: 'Effect of loading frequency on fatigue performance of risers in sour environment', Paper 51641, Offshore Mechanics and Arctic Engineering Conference (OMAE 2004), Vol.III Materials Engineering, ASME, 2004.
8. R I Hammond and D P Baxter, ‘Corrosion fatigue of simulated C-Mn steel HAZ’s in sour produced fluids’, Paper OMAE 2008 - 57149, OMAE 2008 27th international Conference on Offshore Mechanics and Arctic Engineering, Estoril, Portugal, 15 - 20 June 2008.
9. Ramgopal Thodla, Feng Gui, Robin Gordon, Jianjun Xia, “Corrosion Fatigue Performance of Girth Welded X65 Seamless Pipe for Flowline” NACE 2010, San Antonio.
10. M. Kappes, G.S. Frankel, R. Thodla, M.Mueller, N. Sridhar, R. M. Carranza, Accepted for Publication in Corrosion.
11. Compilation of sour service data in literature and various programs that DNV has performed.
12. DNV Internal Data.
13. “Standard Practice for Evaluation of Hydrogen Uptake, Permeation, and Transport in Metals by an Electrochemical Technique,” G148, ASTM International.
14. K. Kiuchi and R. B. Mcllean, Acta Metallurgica, 31(7) 961-984. 1983.
15. A. Turnbull, M. W. Carroll and D. H. Ferriss, Acta Metall. Vol.37, No. 7, 2039-2046, (1989).
16. Magnus Sjellerudsveen, Akselsen Odd Magne, Olden Vigdis, Roy Johnsen, Anna Smirnova. EuroCorr 2010. Moscow: DECHEMA e.V.
17. BSI BS 7448-4: Fracture Mechanics Toughness Tests - Part 4: Method for Determination of Fracture Resistance Curves and Initiation Values for Stable Crack Extension in Metallic Materials.
18. Mohsen Dadfarnia, Brian P. Somerday, Petros Sofronis, Ian M. Robertson, Douglas Stalheim, Journal of Pressure Vessel Technology, 2009, Vol. 131.
19. Ravi Krishnamurthy, “Microstructure and Yield Strength Effects on Hydrogen Environment Fatigue of Steels”, Ph. D. Thesis, University of Virgina, Charlotesville, VA 1991.
20. Zuhair Mattoug Gasem, “Frequency Dependent Environmental Fatigue Crack Propagation in 7xxx Alloy/Aqueous Chloride System”, Ph. D. Thesis, University of Virgina, Charlottesville, VA 1999.
21. R. P. Gangloff, “Science Based Prognosis to Manage Structural Alloy Performance in Hydrogen”.

Table 1

Test matrix for hydrogen flux measurements and the corresponding test environments in which FCGR and FT tests were performed.

©2016 by NACE International.
Requests for permission to publish this manuscript in any form, in part or in whole, must be in writing to
NACE International, Publications Division, 15835 Park Ten Place, Houston, Texas 77084.
The material presented and the views expressed in this paper are solely those of the author(s) and are not necessarily endorsed by the Association.

pH	p_{H2S} (psia)	Sample Type
6	1.2	S135
7	1.2	S135
7	0.12	S135
4	1.2	C110
5	1.2	C110
5	0.12	C110
5	1.2	X80
5	0.12	X80

pH	p_{H2S} (psia)	Sample Type
7	0.12	S135
7	1.2	U165
7	0.12	U165
4	0.12	C110
5	1.2	C110
5	0.12	C110
5	1.2	X80
5	0.12	X80

Table 2

Summary of the results of the hydrogen measurements performed. Binding energy and concentration of the reversible trap sites are also indicated.

pH	p_{H2S} (psia)	Sample Type	D_{eff} (cm^2/s)	J (pL/cm^2-s)	$C_{H,diff}$ (mol/cm^3)	Sample Type	E_b (kJ/mole)	D_O (cm^2/s)	N_l ($site/cm^3$)	N_r ($site/cm^3$)
6	1.2	S135	1.99E-08	1036	1.12E-04	S135	38	7.29E-04	5.23E+23	4.19E+21
7	1.2	S135	6.16E-09	22	7.62E-06	S135	38	7.29E-04	5.23E+23	1.35E+22
7	0.12	S135	1.34E-08	21	3.41E-06	S135	38	7.29E-04	5.23E+23	6.22E+21
6	1.2	U165	1.15E-08	585	1.02E-04	U165	34	7.29E-04	5.23E+23	3.63E+22
6	0.12	U165	1.03E-08	409	8.54E-05	U165	34	7.29E-04	5.23E+23	4.08E+22
7	1.2	U165	6.59E-09	119	3.87E-05	U165	34	7.29E-04	5.23E+23	6.34E+22
7	0.12	U165	6.52E-09	24	7.96E-06	U165	34	7.29E-04	5.23E+23	6.42E+22
4	1.2	C110	4.30E-08	538	2.40E-05	C110	48	7.29E-04	5.23E+23	3.42E+19
4	0.12	C110	4.93E-08	720	2.81E-05	C110	48	7.29E-04	5.23E+23	2.98E+19
5	1.2	C110	6.75E-08	819	2.49E-05	C110	48	7.29E-04	5.23E+23	2.18E+19
5	0.12	C110	5.15E-08	610	2.48E-05	C110	48	7.29E-04	5.23E+23	2.85E+19
4	1.2	X80	1.53E-07	394	1.16E-05	X80	27	7.29E-04	5.23E+23	4.60E+22
4	0.12	X80	1.28E-07	664	2.32E-05	X80	27	7.29E-04	5.23E+23	5.52E+22
5	1.2	X80	1.64E-07	739	2.04E-05	X80	27	7.29E-04	5.23E+23	4.31E+22
5	0.12	X80	1.28E-07	483	1.70E-05	X80	27	7.29E-04	5.23E+23	5.52E+22

Table 3

Summary of R-curve parameters associated with the tests in sour environments for the four different grades of steel.

pH	p_{H2S} (psia)	Sample Type	$J_{0.2mm}$ (N/mm)	$J_{maxload}$ (N/mm)	A (N/mm)	β
7	1.2	S135	6.5	25	19	0.63
7	0.12	S135	131	136	241	0.4
7	1.2	U165	40	106	138	0.56
7	0.12	U165	73	100	190	0.42
5	1.2	C110	30	58	81	0.52
5	0.12	C110	69	87	184	0.48
5	1.2	X80	21	50	71	0.54
5	0.12	X80	25	33	75	0.65

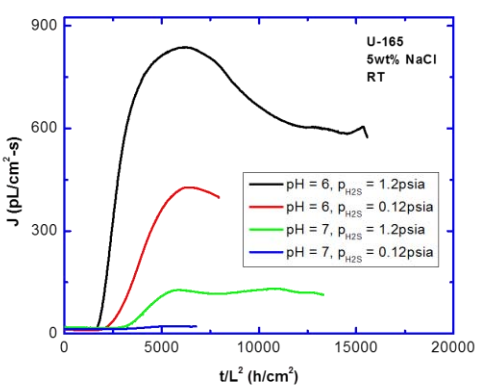

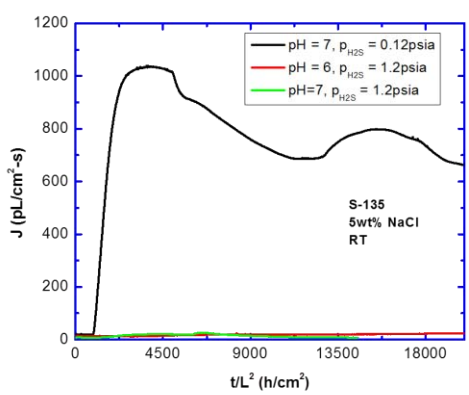

©2016 by NACE International.
Requests for permission to publish this manuscript in any form, in part or in whole, must be in writing to
NACE International, Publications Division, 15835 Park Ten Place, Houston, Texas 77084.
The material presented and the views expressed in this paper are solely those of the author(s) and are not necessarily endorsed by the Association.

Figure 1: Hydrogen flux measurements of UD-165 and S-135 as function of H_2S at pH = 6 and 7.

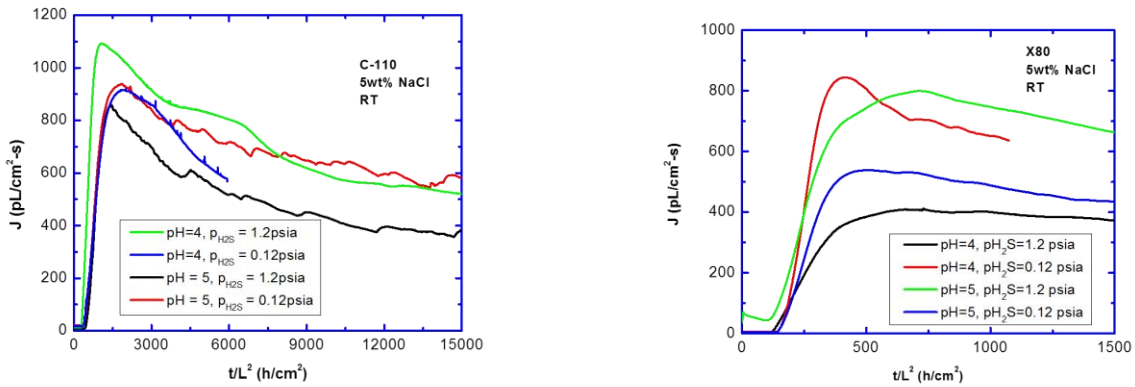

Figure 2: Hydrogen flux measurements on C-110 and X-80 as a function of p_{H2S} at pH = 4 and 5.

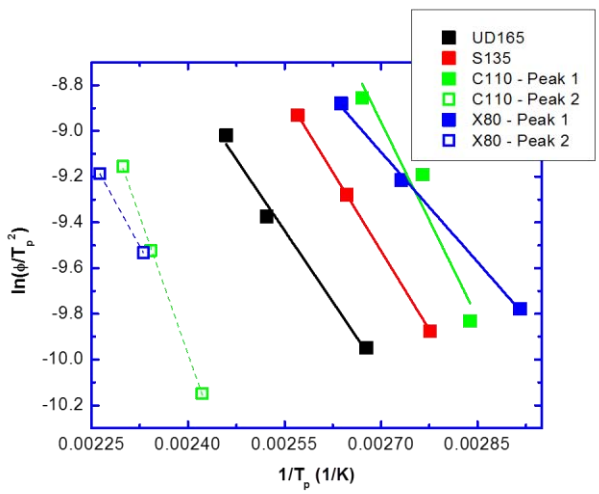

Figure 3: Binding energy of the various steels that were tested.

©2016 by NACE International.
Requests for permission to publish this manuscript in any form, in part or in whole, must be in writing to
NACE International, Publications Division, 15835 Park Ten Place, Houston, Texas 77084.
The material presented and the views expressed in this paper are solely those of the author(s) and are not necessarily endorsed by the Association.

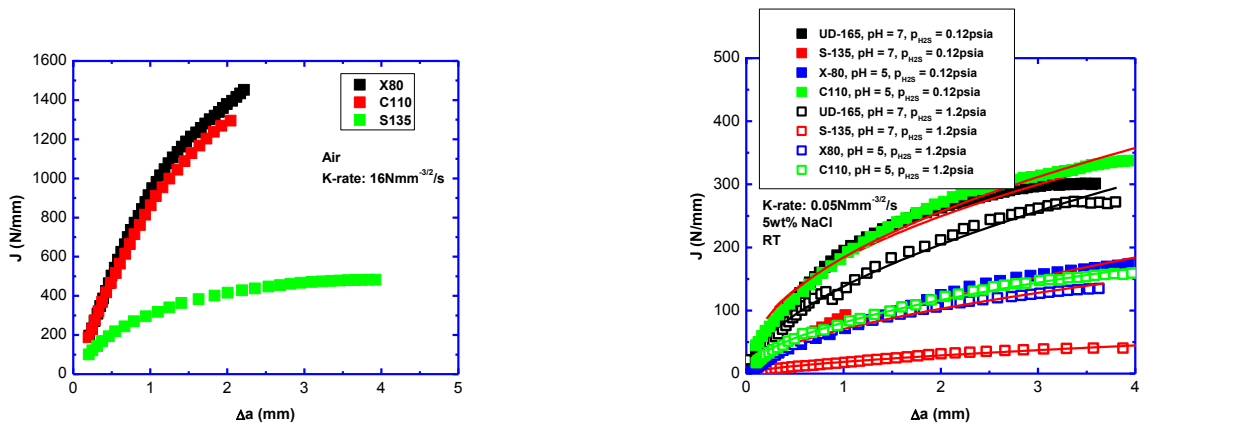

(a) In - Air (b) In environment

Figure 4: J-R curves of three different steels in-air and two different sets of sour environments.

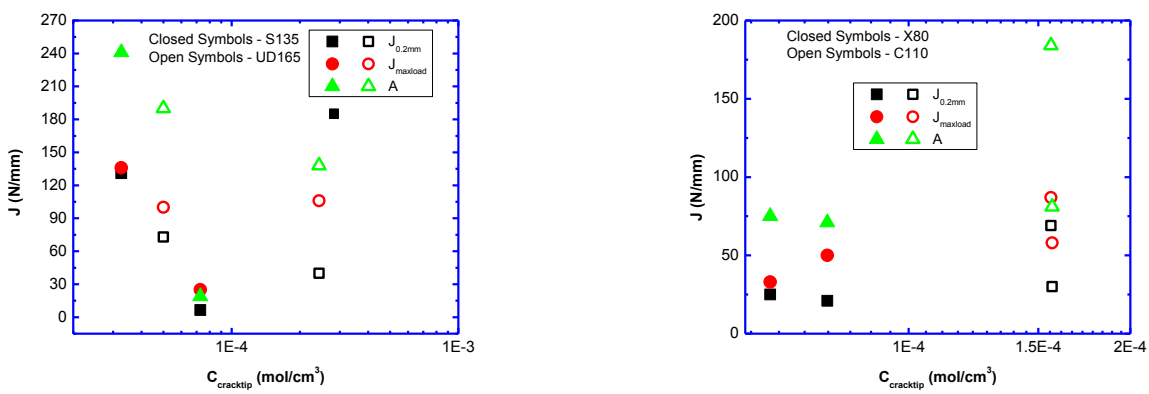

Figure 5: $J_{0.2mm}$, $J_{maxload}$, A for UD-165, S-135, C110, and X-80 as a function of crack tip concentration.

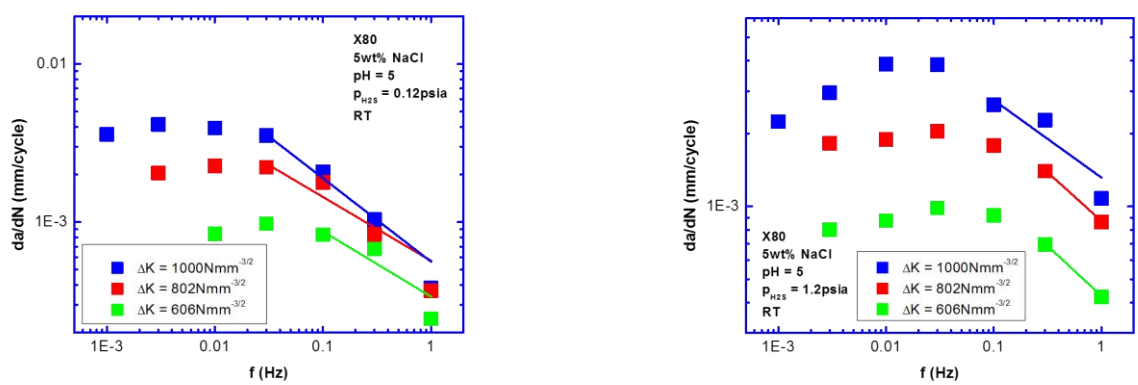

Figure 6: FCGR frequency scans at pH = 5, 0.12psia H_2S on X80 at three different ΔK's.

©2016 by NACE International.
Requests for permission to publish this manuscript in any form, in part or in whole, must be in writing to
NACE International, Publications Division, 15835 Park Ten Place, Houston, Texas 77084.
The material presented and the views expressed in this paper are solely those of the author(s) and are not necessarily endorsed by the Association.

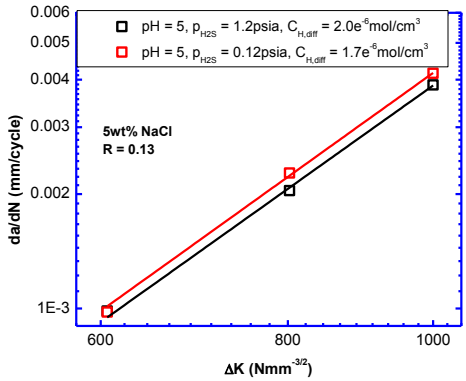

Figure 7: **Plateau FCGR as a function of ΔK for different p_{H2S} for X80.**

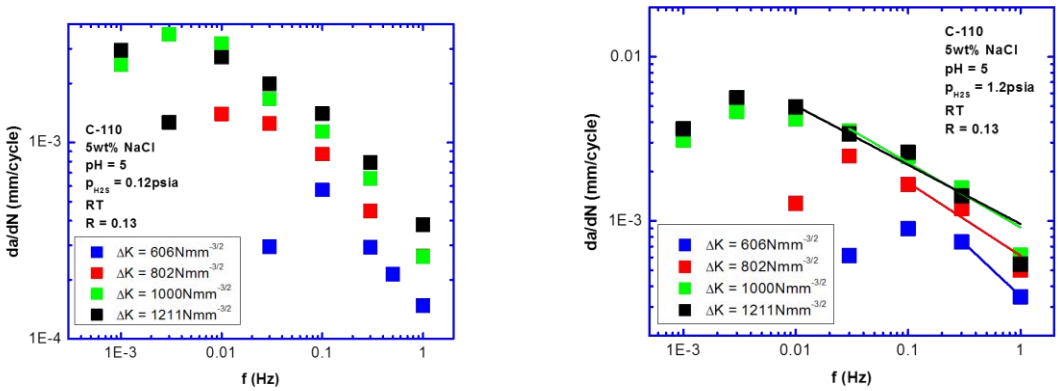

Figure 8: **FCGR frequency scans at pH = 5, 0.12psia and 1.2psia H_2S on C-110 at three different ΔK's.**

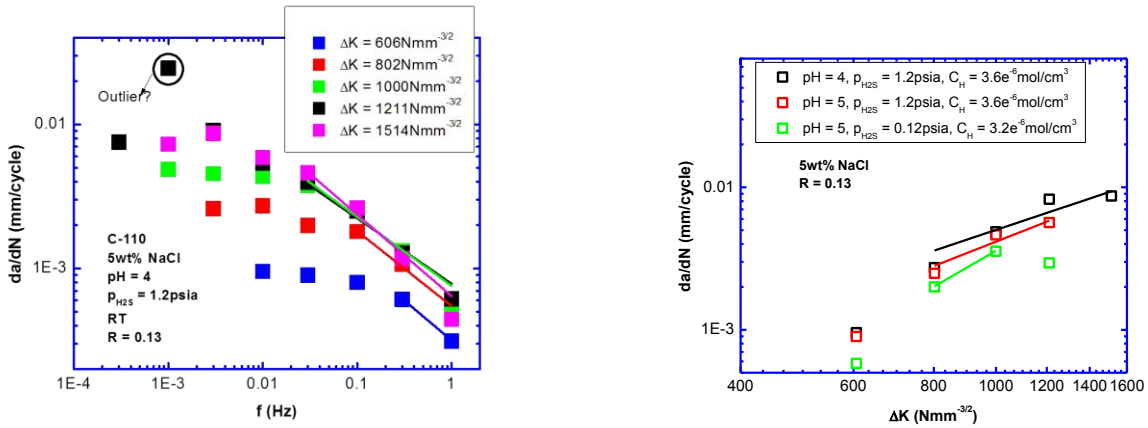

Figure 9: **FCGR frequency scans at pH = 4, 1.2psia H_2S on C-110 at three different ΔK's and the plateau FCGR as a function of ΔK.**

©2016 by NACE International.
Requests for permission to publish this manuscript in any form, in part or in whole, must be in writing to
NACE International, Publications Division, 15835 Park Ten Place, Houston, Texas 77084.
The material presented and the views expressed in this paper are solely those of the author(s) and are not necessarily endorsed by the Association.

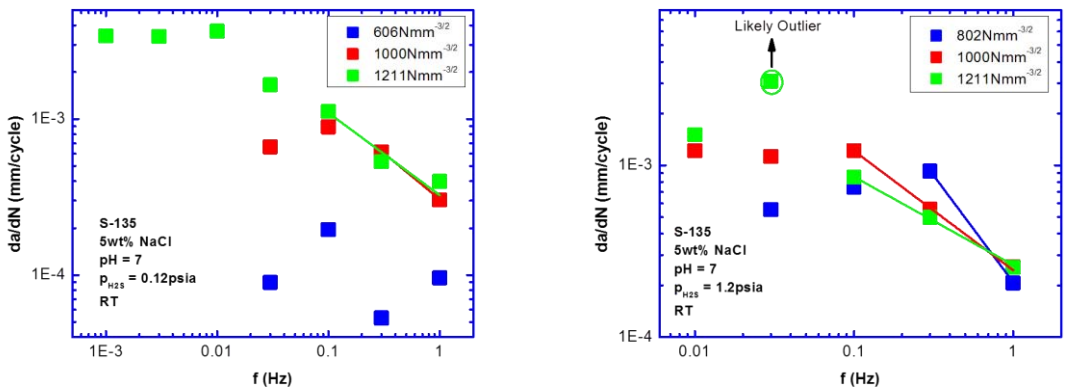

Figure 10: FCGR frequency scans at pH = 7, 0.12psia, 1.2psia H_2S on S-135 at three different ΔK's.

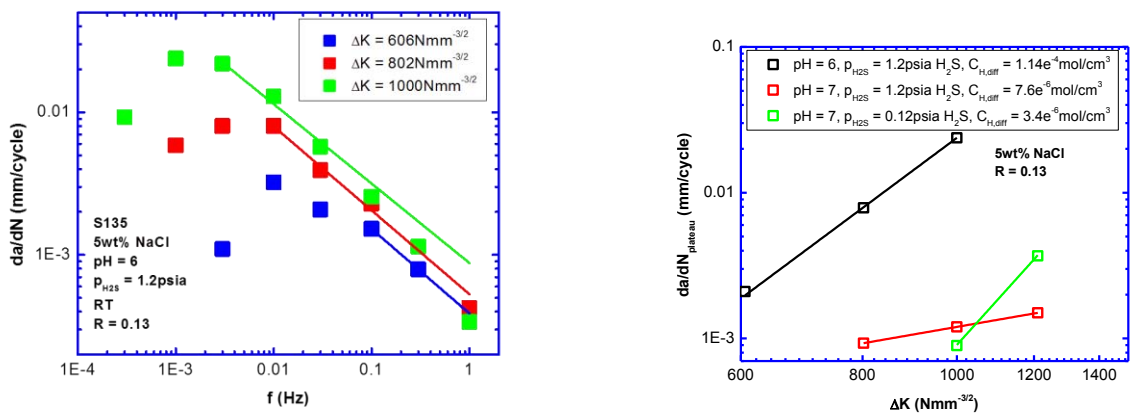

Figure 11: FCGR frequency plots at pH = 6, 1.2psia H_2S on S-135 at three different ΔK's and the plateau FCGR as a function of ΔK.

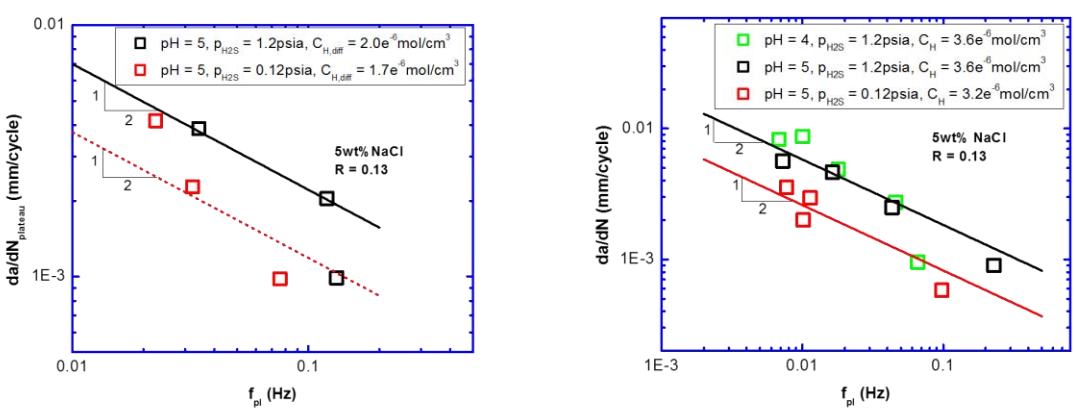

X80 C110

©2016 by NACE International.
Requests for permission to publish this manuscript in any form, in part or in whole, must be in writing to
NACE International, Publications Division, 15835 Park Ten Place, Houston, Texas 77084.
The material presented and the views expressed in this paper are solely those of the author(s) and are not necessarily endorsed by the Association.

Figure 12: **da/dN vs $1/\sqrt{f_{pl}}$ for X80 and C110 over a range of ΔK and hydrogen concentration.**

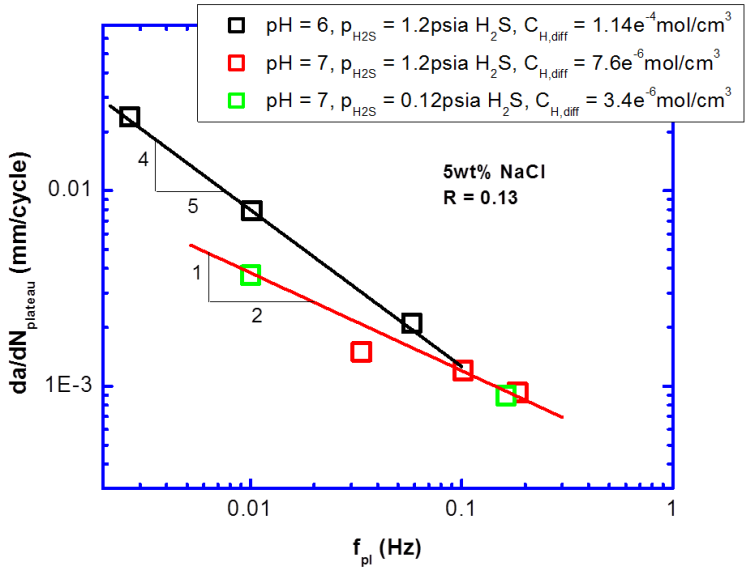

Figure 13: **da/dN vs $1/\sqrt{f_{pl}}$ for S-135 as a function of ΔK in a range of environments.**

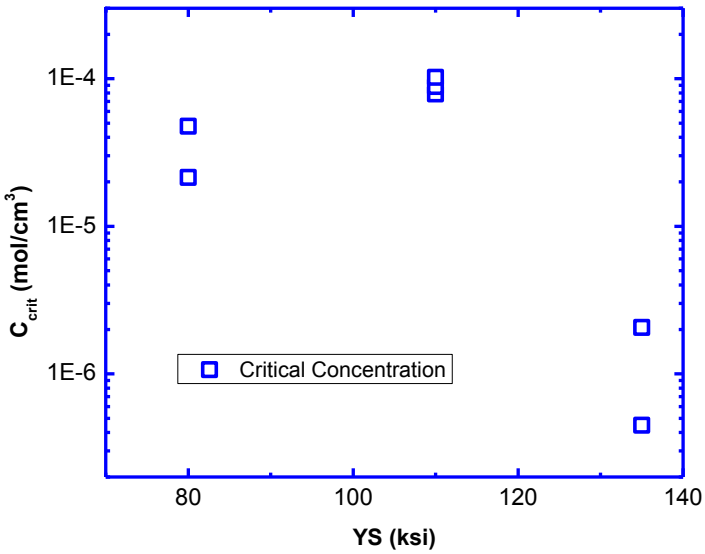

Figure 14: **Critical concentration for crack advance as a function of YS.**

©2016 by NACE International.
Requests for permission to publish this manuscript in any form, in part or in whole, must be in writing to
NACE International, Publications Division, 15835 Park Ten Place, Houston, Texas 77084.
The material presented and the views expressed in this paper are solely those of the author(s) and are not necessarily endorsed by the Association.